

Long-term X-ray variability of the multiple-planet host L 98-59: Hints of an activity cycle.

I. Pillitteri¹, S. Bellotti^{2,3}, S. Benatti¹, S. Boro Saikia⁴, A. García Muñoz⁵, K. G. Kislyakova⁴, A. Maggio¹, G. Micela¹, K. Vida^{6,7}, and A. A. Vidotto²

¹ INAF-Osservatorio Astronomico di Palermo, Piazza del Parlamento 1, 90134 Palermo, Italy
e-mail: ignazio.pillitteri@inaf.it

² Leiden Observatory, Leiden University, PO Box 9513, 2300 RA Leiden, The Netherlands

³ Institut de Recherche en Astrophysique et Planétologie, Université de Toulouse, CNRS, IRAP/UMR 5277, 14 avenue Edouard Belin, F-31400, Toulouse, France

⁴ Department of Astrophysics, University of Vienna, Türkenschanz Strasse 17, 1180, Vienna, Austria

⁵ Université Paris-Saclay, Université Paris Cité, CEA, CNRS, AIM, Gif-sur-Yvette, 91191, France

⁶ Konkoly Observatory, HUN-REN Research Centre for Astronomy and Earth Sciences, Konkoly Thege Miklós út 15-17., H-1121, Budapest, Hungary

⁷ HUN-REN CSFK, MTA Centre of Excellence, Budapest, Konkoly Thege Miklós út 15-17., H-1121, Budapest, Hungary

Received; accepted

ABSTRACT

High-energy irradiation in X-rays and UV (XUV) can transform the planetary atmospheres through photoevaporation and photochemistry. This is more crucial for M stars, whose habitable zones for Earth-like planets are located within a few percent of an AU. Transiting exoplanets around M dwarfs offer the opportunity to study their characteristics and habitability conditions. L 98-59 is an M3 dwarf hosting six Earth-like planets, with two of them in the habitable zone of the star. X-ray observations made in 2020 and 2021 detected significant flares above a quiescent luminosity of $4 - 10 \times 10^{26} \text{ erg s}^{-1}$. We present the results from two short *XMM-Newton* observations of L 98-59, which are part of a monitoring survey to detect long-term X-ray variability and activity cycles. In October 2024 the X-ray quiescent luminosity of the star was $\sim 5.9 \times 10^{25} \text{ erg s}^{-1}$, and it was about $6.3 \times 10^{26} \text{ erg s}^{-1}$ in February 2025. We speculate that in late 2024 the star had a minimum of activity; in 2021 the star was near a maximum of an activity cycle, and in 2025 it was at the middle of the cycle. We suggest a coarse estimate of the period of ≈ 2 years and a peak-to-peak amplitude of about ≈ 10 , which is the highest among the stars with a known X-ray cycle other than the Sun. We also infer that even the outer planet in the habitable zone, L 98-59f, is exposed to an X-ray dose between 100 and 1600 times the X-ray irradiation of the Earth in the XMM band.

Key words. stars: activity – stars: coroneae – stars: low-mass – (stars:) planetary systems – stars: individual:: L 98-59

1. Introduction

The discovery of the solar magnetic activity cycle—revealed by periodic variations in sunspot numbers—was one of the earliest astrophysical milestones (Schwabe 1844). Similar chromospheric cycles have since been detected in many stars through long-term Ca II H&K monitoring (e.g., Baliunas et al. 1995), with periods ranging from months to decades. However, the high-energy counterpart of these cycles, in X-rays, remains poorly explored. To date, only seven stars are known to host X-ray cycles (e.g., Robrade & Schmitt 2016; Coffaro et al. 2020, 2022).

The scarcity of detections reflects the challenges of X-ray monitoring, but also represents a major gap in our understanding. X-ray emission traces the hot corona and dominates the high-energy irradiation of exoplanets. Its variability on cycle timescales can strongly influence atmospheric evaporation and photochemistry, processes that ultimately determine the fate of planetary atmospheres. However, whether X-ray cycles follow the same behavior as chromospheric cycles, and how their amplitude and timescales depend on stellar age and type, remain open questions. The aim of our program is to close this gap with the first systematic, multi-year monitoring of a well-characterized stellar

sample. By focusing on transiting-planet hosts in the Ariel Mission Reference Sample, the results can have a relevant impact on exoplanet atmosphere studies.

Photoevaporation and photochemistry processes among exoplanets are determined by the high-energy stellar irradiation in X-ray and EUV (XUV) bands, the stellar activity and the frequency of XUV flares, and Coronal Mass Ejections (CMEs). The effects of long timescale modulation of XUV irradiation are still to be understood due to the sparse knowledge of stellar cycles in the XUV band (Jeffers et al. 2023).

While the search for chromospheric activity cycles in stars received a strong impulse by the monitoring operated at the Mount Wilson Observatory between 1966 and 1995¹ (Vaughan et al. 1978; Wilson et al. 1981), in X-rays there are very few cycles detected among FGK stars because of the sparse observations. X-ray cycles have been found in Alpha Cen A & B (Robrade & Schmitt 2016), Prox Cen (Wargelin et al. 2024), 61 Cyg A & B (Hempelmann et al. 2006; Robrade et al. 2012), HD 81809 (Favata et al. 2008; Orlando et al. 2017), ι Hor (Sanz-Forcada et al. 2013), ϵ Eri (Coffaro et al. 2020), and Kepler 63

¹ https://dataverse.harvard.edu/dataverse/mwo_hk_project

(Coffaro et al. 2022). From this small sample, it emerges that X-ray cycles have shorter periods and smaller peak-to-peak amplitudes in younger stars (Favata et al. 2008), and this behavior could be ascribed to a larger filling factor of active regions in the coronae with higher levels of activity. In 61 Cyg A the periods of chromospheric and X-ray cycles are similar to those of the Sun (Boro Saikia 2016; Boro Saikia et al. 2018). A short cycle of 122 days has been detected in τ Bootis in the chromospheric and optical bands (Mittag et al. 2017; Jeffers et al. 2018) in rough agreement with a similar cycle found in X-rays. Also worth noting is the 1.6-year chromospheric cycle found in ι Hor (age $t \sim 0.6$ Gyr), which also shows a beating pattern (Alvarado-Gómez et al. 2018). Peculiarly, in ϵ Eri the X-ray and chromospheric cycles did not follow the same trend (Coffaro et al. 2020), suggesting that X-ray cycles can behave differently from chromospheric cycles for reasons that are not yet understood.

We embarked on a monitoring survey with *XMM-Newton* of a selected list of targets for the ESA Ariel mission (Tinetti et al. 2018). The aim was to discover more X-ray cycles among planet hosts and to determine whether these cycles can have any effects on the atmospheres of their planets. Knowing the X-ray cycle could help to plan the optical observations of planetary atmospheres during the low-activity phases, thus minimizing the effects related to the stellar activity. Similar efforts for Ariel have also been conducted from ground-based spectropolarimetric observations (Bellotti et al. 2024). Here we present the first two observations from our program targeting L 98-59 (TOI-175), which is an M3 dwarf at 10.6 pc from the Sun (Cloutier et al. 2019). The system of L 98-59 is composed of at least six planets with masses between $0.4 M_{\oplus}$ and $3 M_{\oplus}$; planets *e* and *f* are in the habitable zone, and planet *d* likely possesses water and a gaseous envelope (Demangeon et al. 2021). L 98-59 has also been a target of JWST transmission spectroscopy; sulfur was detected in the atmosphere of the $1.6 M_{\oplus}$ planet *d* (Gressier et al. 2024). Transiting planets around M dwarfs similar to L 98-59 are particularly appealing since their putative habitable zones are within a few tenths of AU, corresponding to periods of a few days. They are thus suitable for transmission spectroscopy and atmospheric composition retrieval. L 98-59 thus constitutes an important system for the study of the habitability of the extrasolar planets around M stars in the solar neighborhood. Together with similar nearby M dwarfs with packed planetary systems, for example Trappist-1 and LHS 1140, L 98-59 is thus a prime target for the characterization of Earth-like planets with present and future observatories such as JWST and Ariel.

The structure of the paper is the following. Section 2 describes the *XMM-Newton* observations and their analysis. In Section 3 we present our results. In Section 4 we discuss the results and give our conclusions.

2. Observations

L 98-59 was observed with *XMM-Newton* in three previous epochs (see Table A.1). In those observations the quiescent luminosity was about $4 - 10 \times 10^{26}$ erg s $^{-1}$ in the band 0.3 – 10 keV. The star showed two prominent flares (cf. Fig. A.1; see Behr et al. 2023), which is a typical signature of X-ray activity in M stars.

Here we present the results of two further observations targeting L 98-59, together with a re-analysis of the archival observations in a homogeneous way (see Sect. A). We also made use of archival optical spectra of L 98-59 to infer the chromospheric activity index $\log R'_{HK}$ (see Sect. B).

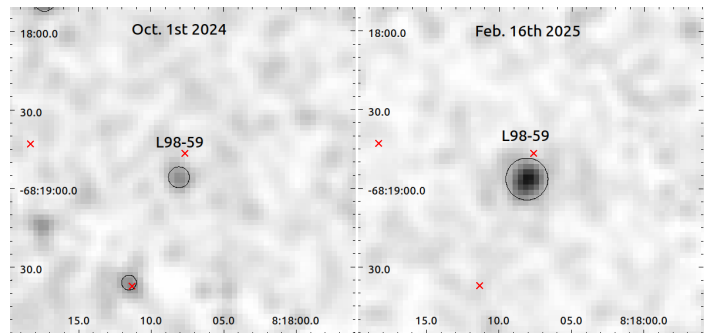


Fig. 1. Comparison of X-ray rate images. The red crosses mark the positions of the objects in SIMBAD. L 98-59 has high proper motions toward the bottom left of the image and its current position is coincident with the centroid of the X-ray emission. The images are on the same pixel and color intensity scales (2"/pix, maximum 2.5 counts per pixel) and are smoothed with a Gaussian kernel with $\sigma = 1.5$ pixels.

3. Results

L 98-59 was detected in both our *XMM-Newton* observations in October 2024 and February 2025, but with different significance over the local background mean level. In particular the significance was about 5.3σ in October 2024, while the significance of the source was about 13.3σ in February 2025. In previous observations it was detected with a significance level comprised between 12.1 and 20.3σ . The flux and luminosity of L 98-59 in 2024 was a factor of five to ten lower than the corresponding quiescent rate recorded in the other observations. If we also consider the peaks of the flares recorded in 2021 (Behr et al. 2023) the difference with the lowest quiescent emission is about a factor 100. The hardness ratio obtained from *pn* counts in the bands 0.3 – 0.7 keV and 0.7 – 8.0 keV shows a quite soft spectrum; there is a shallow positive trend of the spectral hardness with the flux, but its significance is affected by the low count statistics. In general, however, an intrinsically harder spectrum is expected for higher flux emitted from hotter plasma.

A low level of activity and the X-ray emission from the corona and its soft spectrum inferred from the hardness ratio supports a very old age for L 98-59. The decrease in flux across the X-ray observations is likely associated with an overall decrease in the emission measure of the plasma in terms of volume of emitting plasma and number of coronal active regions. This means that in 2024 the corona of L 98-59 was devoid of significant active regions, similarly to the Sun at its minimum of activity. The star shows some degree of variability in X-rays even at its lowest level of emission, but owing to the low count statistics the variability is within 3σ of the mean count rate (Fig. A.1).

4. Discussion and conclusions

In a 10 ks *XMM-Newton* observation of L 98-59 obtained in October 2024 we detected an X-ray flux that was about ten times lower than the flux measured in the other observations, with a significance of more than 3σ . In February 2025 the flux was between the values recorded in 2020 and in 2021 (Fig. 2).

We speculate that an activity cycle in X-rays could be at work in L 98-59 with a period of about 2 years (Fig. 2), although we are aware that more monitoring is required to firmly detect such a cycle. The star was near its minimum of activity during late 2024 and had a maximum of activity presumably in mid-2021 (and another unmeasured peak in 2023) plus intermediate states recorded in December 2020 and February 2025. Near the max-

Table 1. Count rates, detection significance, unabsorbed X-ray flux and luminosity, and hardness ratio (HR) of L 98-59 in each of the *XMM-Newton* observations during the quiescent intervals.

ObsID	Year	Exp. time (ks)	Signif. σ	SAS_ML	Rate 10^{-3} ct s $^{-1}$	f_X 10^{-14} erg s $^{-1}$ cm $^{-2}$	L_X 10^{26} erg s $^{-1}$	HR
0863400601	2020	27.2	15.6	100.16	3.93 ± 0.53	3.06 ± 0.41	4.13 ± 0.6	-0.12 (-0.60 – 0.32)
0871800201	2021	11.6	17.3	159.25	9.87 ± 1.21	7.66 ± 0.80	10.34 ± 1.1	0.14 (-0.20 – 0.46)
0871800301	2021	10.2	12.1	65.9	7.78 ± 1.26	6.05 ± 0.77	8.16 ± 1.05	0.08 (-0.39 – 0.50)
(087180-Sum	2021	21.8	20.3	–	7.84 ± 0.82	6.10 ± 0.98	8.23 ± 1.32	0.11 (-0.15 – 0.38)
0940540301	2024	34.0	5.3	11.44	0.56 ± 0.16	0.44 ± 0.13	0.59 ± 0.17	-0.27 (-1.00 – 0.53)
0940540401	2025	15.6	13.3	110.48	6.0 ± 0.9	4.71 ± 0.67	6.33 ± 0.9	-0.04 (-0.37 – 0.261)

Notes. Exposure time is the sum of MOS and pn exposure times in quiescent intervals. Significance is in units of σ of local background. SAS_ML is the maximum likelihood value of the source detection performed with SAS. Count rates are scaled to the MOS effective area. Unabsorbed fluxes in 0.3–10 keV band were determined assuming a 1T APEC thermal model with solar abundances, $kT = 0.17$ keV and $N_H = 10^{18}$ cm $^{-2}$. Luminosities are calculated assuming a distance of 10.6 pc. HR calculated from pn counts in the bands $S = 0.3 - 0.7$ keV (soft) and $H = 0.7 - 8.0$ keV (hard). We report the measurements from the sum of the observations 0871800201 and 0871800301.

imum the star was characterized by frequent flaring activity together with a higher basal X-ray emission (see Behr et al. 2023).

L 98-59 was detected by eROSITA in the eRASS1 catalog (Merloni et al. 2024) with a $\log L_X = 26.48$ and a ratio $\log L_X/L_{\text{bol}} = -5.14$. The luminosity from eROSITA is similar to the *XMM-Newton* luminosity measured in 2020.

Boro Saikia et al. (2018) reported measurements of $\log R'_{\text{HK}}$ for 4454 stars along the main sequence from F to M dwarfs. We compare the 5%-95% quantile range variation of L 98-59 with their sample in Fig. 3. At $\log R'_{\text{HK}} = -5.6$, which corresponds to the 5% quantile, the star is one of the most inactive in the sample of M dwarfs, and when $\log R'_{\text{HK}}$ reaches the 95% quantile at ~ -5.2 the star appears more similar to the other M dwarfs.

Overall, the star looks very old and inactive; an estimate of the age based on its rotation period and $\log R'_{\text{HK}}$ points to $t \geq 5$ Gyr (Boudreaux et al. 2022; Engle & Guinan 2023). Compared to other mid-M stars with a similar rotation period of 80 days, L 98-59 lies at the bottom of the X-ray luminosity distribution when it is at the minimum of activity (cf. Fig. 2 in Magaúda et al. 2020).

L 98-59 would be the second M dwarf with a potential activity cycle in X-rays together with Prox Cen (Wargelin et al. 2017, 2024). Prox Cen and L 98-59 have similar rotation periods (89 days vs. 80 days, Medina et al. 2020), the spectral type of Prox Cen is later than that of L 98-59. However, while the X-ray cycle in Prox Cen has an amplitude of a factor of 1.5, in L 98-59 the amplitude could be larger as it does show a peak-to-peak amplitude of a factor of about ten. The other known stars with X-ray cycles are either G or K stars, often members of binary systems.

Coffaro et al. (2022, Fig. 20) compared the X-ray surface fluxes and ages of stars with cycles with the amplitude of their X-ray cycles ($L_{X,\text{max}}/L_{X,\text{min}}$) noting that higher fluxes due to young age and higher activity correspond to cycles with lower amplitudes or absent cycles. L 98-59 is consistent with the empirical relationship obtained by Coffaro et al. (2022) only when the star is at its lowest activity level, with a surface X-ray flux of about 10^4 erg s $^{-1}$ cm $^{-2}$ and for an age of $t \geq 5$ Gyr, while it appears a strong outlier when it is at the maximum of activity bearing an X-ray surface flux one order of magnitude higher.

In the absence of an activity cycle, the sharp drop in luminosity could be attributed to a corona with a more active X-ray bright side and a less active X-ray dark side. However, there is a low probability that such a dark side would have been spotted in only one short exposure out of five observations. The interpretation that there is an activity cycle appears the most viable;

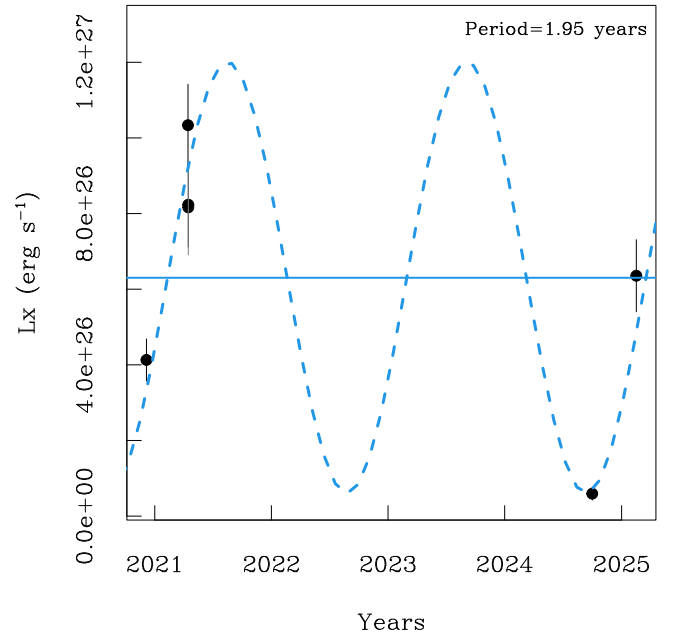


Fig. 2. X-ray luminosity of L 98-59 in the band 0.3-10 keV vs. time. A cycle of about 1.95 years is shown as a sinusoidal dashed line. We made a rough estimate of the period by assuming that the minimum of the sinusoid is the value recorded in October 2024 and that its mean is equal to the value measured in February 2025.

however more monitoring is needed to determine the nature of the X-ray variability of L 98-59 that we observed on a timescale of a few months.

The X-ray hardness ratio of L 98-59 across the observations has a slight trend, but overall it is the feature of a steady soft spectrum during the quiescent phases. The low flux recorded in 2024 could be due to a low plasma emission measure in an X-ray dark corona devoid of active regions. In this configuration, a steady stellar wind would originate from an open magnetic field line configuration. The maximum of activity instead would be characterized by frequent flares (Fig. A.1) and perhaps CMEs occurring during the most powerful events. In this phase of the cycle the corona would be composed of X-ray bright active regions with a closed magnetic field. These two different configurations can have an impact on the dynamics and chemistry of

Table 2. XUV (5-920 Å) fluxes in log scale received from planets b–e at three different levels of XUV luminosity.

planet d (AU)	b	c	d	e	f	g
	0.0219	0.0304	0.0486	0.0717	0.1053	0.0188
$\log L_{\text{XUV}} \text{ (erg s}^{-1}\text{)}$	$\log f_{\text{XUV}} \text{ (erg s}^{-1}\text{ cm}^{-2}\text{)}$					
27.03	2.90	2.62	2.21	1.87	1.54	3.03
28.06	3.93	3.64	3.24	2.90	2.57	4.06
28.26	4.13	3.84	3.44	3.10	2.77	4.26

Notes. The separation adopted for flux calculation is listed under each planet.

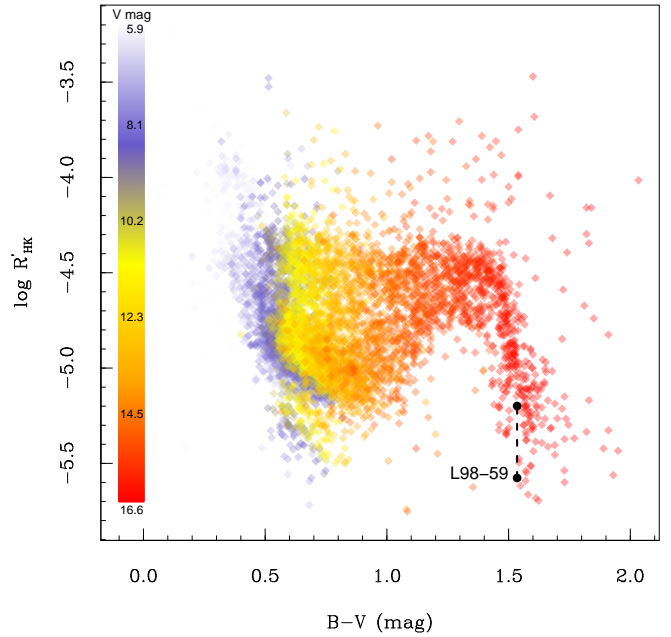
the atmospheres of the planets around L 98-59. The steady stellar wind could erode the planetary atmospheres on timescales of several hundreds of megayears or gigayears, while flares and CMEs can both produce effects on short timescales related to heating, evaporation, high-energy particle interaction, and photochemistry.

We calculated the irradiation of the planets in the XUV band 5 – 920 Å for different levels of X-ray luminosity of the host star (Table 2). The EUV luminosity in 100 – 920 Å was estimated to be about ten times the X-ray luminosity in the ROSAT band (see Fig. 3 in Sanz-Forcada et al. 2025). The XUV flux varies between ~ 34 and $18,200 \text{ erg s}^{-1} \text{ cm}^{-2}$ across the six planets. For reference, the Earth’s X-ray irradiation is about $0.35 \text{ erg s}^{-1} \text{ cm}^{-2}$ in the same band. Even the outer planet *f* orbiting in the habitable zone of L 98-59 is exposed to an XUV dose between 100 and 1600 times the X-ray irradiation of the Earth. Such irradiation can produce several effects, for example photodissociation, photoionization, photochemical reactions, deposits of heating due to scattered secondary electrons, and evaporation (see Cecchi-Pestellini et al. 2006). In extreme cases planets can lose their atmospheres due to intense irradiation acting for several gigayears (Lammer et al. 2003; Fromont et al. 2024; Van Looveren et al. 2025). Highly X-ray irradiated upper atmospheres can exhibit signatures of molecular lines in the near-IR, which can be probed by NASA JWST now, and will be probed by ESA Ariel in the near future (Cecchi-Pestellini et al. 2009; Locci et al. 2024).

Acknowledgements. IP acknowledges support from Bando per il Finanziamento della Ricerca Fondamentale 2024 dell’Istituto Nazionale di Astrofisica (INAF). AM and GM acknowledge support from the European Union - Next Generation EU through the grant n. 2022J7ZFRA - Exo-planetary Cloudy Atmospheres and Stellar High energy (Exo-CASH), funded by MUR-PRIN 2022, and the ASI-INAF agreement 2021-5-HH.2-2024. AAV acknowledges funding from the European Research Council (ERC) under the European Union’s Horizon 2020 research and innovation programme (grant agreement No 817540, ASTROFLOW) and funding from the Dutch Research Council (NWO), with project number VIC.232.041 of the Talent Programme Vici. KV acknowledges the support of the Hungarian National Research, Development and Innovation Office (NKFIH) Élvonal grant KKP 143986. SB acknowledges funding by the Dutch Research Council (NWO) under the project “Exo-space weather and contemporaneous signatures of star-planet interactions” (with project number OCENW.M.22.215 of the research programme “Open Competition Domain Science- M”). Based on observations obtained with XMM-Newton, an ESA science mission with instruments and contributions directly funded by ESA Member States and NASA. Based on observations collected at the European Southern Observatory under ESO programs 1102.C-0339(A), 0102.C-0525 and 0102.D-0483, 1102.C-0744, 1102.C-0958 and 1104.C-0350. This work made use of data from eROSITA, a joint German-Russian science mission with the support of the Deutsches Zentrum für Luft- und Raumfahrt (DLR).

References

Alvarado-Gómez, J. D., Hussain, G. A. J., Drake, J. J., et al. 2018, *MNRAS*, 473, 4326

**Fig. 3.** Index $\log R'_{\text{HK}}$ for F to M dwarfs from Boro Saikia et al. (2018) and the range of $\log R'_{\text{HK}}$ observed in L 98-59.

- Astudillo-Defru, N., Delfosse, X., Bonfils, X., et al. 2017, *A&A*, 600, A13
 Behr, P. R., France, K., Brown, A., et al. 2023, *AJ*, 166, 35
 Bellotti, S., Evensberger, D., Vidotto, A. A., et al. 2024, *A&A*, 688, A63
 Boro Saikia, S. 2016, PhD thesis, Georg August University of Göttingen, Germany
 Boro Saikia, S., Marvin, C. J., Jeffers, S. V., et al. 2018, *A&A*, 616, A108
 Boudreaux, E. M., Newton, E. R., Mondrik, N., Charbonneau, D., & Irwin, J. 2022, *ApJ*, 929, 80
 Cecchi-Pestellini, C., Ciaravella, A., & Micela, G. 2006, *A&A*, 458, L13
 Cecchi-Pestellini, C., Ciaravella, A., Micela, G., & Penz, T. 2009, *A&A*, 496, 863
 Cloutier, R., Astudillo-Defru, N., Bonfils, X., et al. 2019, *A&A*, 629, A111
 Coffaro, M., Stelzer, B., & Orlando, S. 2022, *A&A*, 661, A79
 Coffaro, M., Stelzer, B., Orlando, S., et al. 2020, *A&A*, 636, A49
 Damiani, F., Maggio, A., Micela, G., & Sciortino, S. 1997a, *ApJ*, 483, 350
 Damiani, F., Maggio, A., Micela, G., & Sciortino, S. 1997b, *ApJ*, 483, 370
 Demangeon, O. D. S., Zapatero Osorio, M. R., Alibert, Y., et al. 2021, *A&A*, 653, A41
 Engle, S. G. & Guinan, E. F. 2023, *ApJ*, 954, L50
 Favata, F., Micela, G., Orlando, S., et al. 2008, *A&A*, 490, 1121
 Fromont, E. F., Ahlers, J. P., do Amaral, L. N. R., et al. 2024, *ApJ*, 961, 115
 Gressier, A., Espinoza, N., Allen, N. H., et al. 2024, *ApJ*, 975, L10
 Hempelmann, A., Robrade, J., Schmitt, J. H. M. M., et al. 2006, *A&A*, 460, 261
 Jeffers, S. V., Kiefer, R., & Metcalfe, T. S. 2023, *Space Sci. Rev.*, 219, 54
 Jeffers, S. V., Mengel, M., Moutou, C., et al. 2018, *MNRAS*, 479, 5266
 Lammer, H., Selsis, F., Ribas, I., et al. 2003, *ApJ*, 598, L121
 Locci, D., Aresu, G., Petralia, A., et al. 2024, *The Planetary Science Journal*, 5, 58
 Magaúda, E., Stelzer, B., Covey, K. R., et al. 2020, *A&A*, 638, A20
 Medina, A. A., Winters, J. G., Irwin, J. M., & Charbonneau, D. 2020, *ApJ*, 905, 107
 Merloni, A., Lamer, G., Liu, T., et al. 2024, *A&A*, 682, A34
 Mittag, M., Robrade, J., Schmitt, J. H. M. M., et al. 2017, *A&A*, 600, A119
 Noyes, R. W., Hartmann, L. W., Baliunas, S. L., Duncan, D. K., & Vaughan, A. H. 1984, *ApJ*, 279, 763
 Orlando, S., Favata, F., Micela, G., et al. 2017, *A&A*, 605, A19
 Robrade, J., & Schmitt, J. H. M. M. 2016, arXiv e-prints, arXiv:1612.06570
 Robrade, J., Schmitt, J. H. M. M., & Favata, F. 2012, *A&A*, 543, A84
 Sanz-Forcada, J., López-Puertas, M., Lampón, M., et al. 2025, *A&A*, 693, A285
 Sanz-Forcada, J., Stelzer, B., & Metcalfe, T. S. 2013, *A&A*, 553, L6
 Tinetti, G., Drossart, P., Eccleston, P., et al. 2018, *Experimental Astronomy*, 46, 135
 Van Looveren, G., Boro Saikia, S., Herbort, O., et al. 2025, *A&A*, 694, A310
 Vaughan, A. H., Preston, G. W., & Wilson, O. C. 1978, *PASP*, 90, 267
 Wargelin, B. J., Saar, S. H., Irving, Z. A., et al. 2024, *ApJ*, 977, 144
 Wargelin, B. J., Saar, S. H., Pojmański, G., Drake, J. J., & Kashyap, V. L. 2017, *MNRAS*, 464, 3281
 Wilson, O. C., Vaughan, A. H., & Mihalas, D. 1981, *Scientific American*, 244, 104

Appendix A: XMM-Newton data analysis

We observed L 98-59 with *XMM-Newton* on October 1st 2024 and on February 16th 2025 with EPIC as prime instrument (see Table A.1 for the details). The files constituting the observation were downloaded and reduced with SAS 21 and SAS 22 to obtain tables of the events recorded by the EPIC cameras MOS and *pn*. The background rate was low during the first observation and it did not require further time filtering. In contrast, background flaring, due to space weather conditions, was severe during the second exposure and thus we filtered out the high background intervals. We retained the events in the band 0.3 – 10 keV, with FLAG == 0 and PATTERN <= 12. Due to the close distance and the high proper motions of the star, the actual sky coordinates of L 98-59 and the centroid of the X-ray emission are offset with respect to the J2000 coordinates by about 8". We also acquired images with the OM and the filter UVM2, however the star was not detected in this band (200 – 300 nm). Light curves were produced with SAS tasks *evselect* and *epiccorr* and they are shown in Fig. A.1.

At a visual inspection, the star was barely noticeable in the observation of October 2024 while it was brighter in February 2025 and in the observations made in 2020 and 2021 (Fig. 1). We performed a source detection process with a wavelet convolution based code tailored for *XMM-Newton* (Damiani et al. 1997a,b) in order to estimate the count rate the band 0.3 – 10 keV. The code performs a wavelet convolution and find the peaks of the wavelet convolved image from which it derives the count rate of the sources in the initial rate image. A feature of the code is the ability to sum several EPIC images from MOS and *pn* within an offset of about 7" in order to get the deepest sensitivity. To do so, exposure maps of each MOS and *pn* at a resolution of 2" were built with SAS and values of the effective area weighted for a thermal spectrum were used to properly scale the counts of each EPIC instrument. We analyzed the sum of the rate images properly scaled for the effective area of each EPIC camera. The code output consists of a list of detected sources with positions, count rates and detection significance, a combined event list from the input files, a rate image, and background and exposure maps. The resulting count rates are listed in Table 1.

For the archival observations we selected the quiescent emission in the pre-flare intervals for the observations by France (2030 s for Obsid 0871800201 and 2400s for 0871800301), and the middle interval for the observation by Wolk. Figure A.1 shows the intervals used for the quiescent emission. We analyzed the resulting images with the same wavelet convolution procedure to obtain the rates and the detection significance listed in Table 1. The final count rates are scaled to the MOS instrument sensitivity. From count rates we obtained fluxes using the PIMMS software. We adopted a 1T thermal APEC model with plasma at $\log T = 6.3$ or $kT = 0.17$ keV, solar abundances and $N_H = 10^{18} \text{ cm}^{-2}$. The choice is consistent with the best fit of the quiescent spectrum acquired in 2021 (Behr et al. 2023). From fluxes we obtained luminosity values using the distance of 10.6 pc to the star. From *pn* events we derived also a hardness ratio $HR = (H - S)/(H + S)$ by selecting events in 0.3 – 0.7 keV for the soft band and 0.7-8.0 keV for the hard band. The values for each observation are listed in Table 1.

As a further check on the variability of the star in X-rays, we performed the source detection with SAS ver. 22 with the *edetect_chain* task which operates a detection based on the smoothed image with a *boxcar* function and a maximum likelihood (ML) estimate of detection on the final list of detected sources. This task however does not allow to combine images

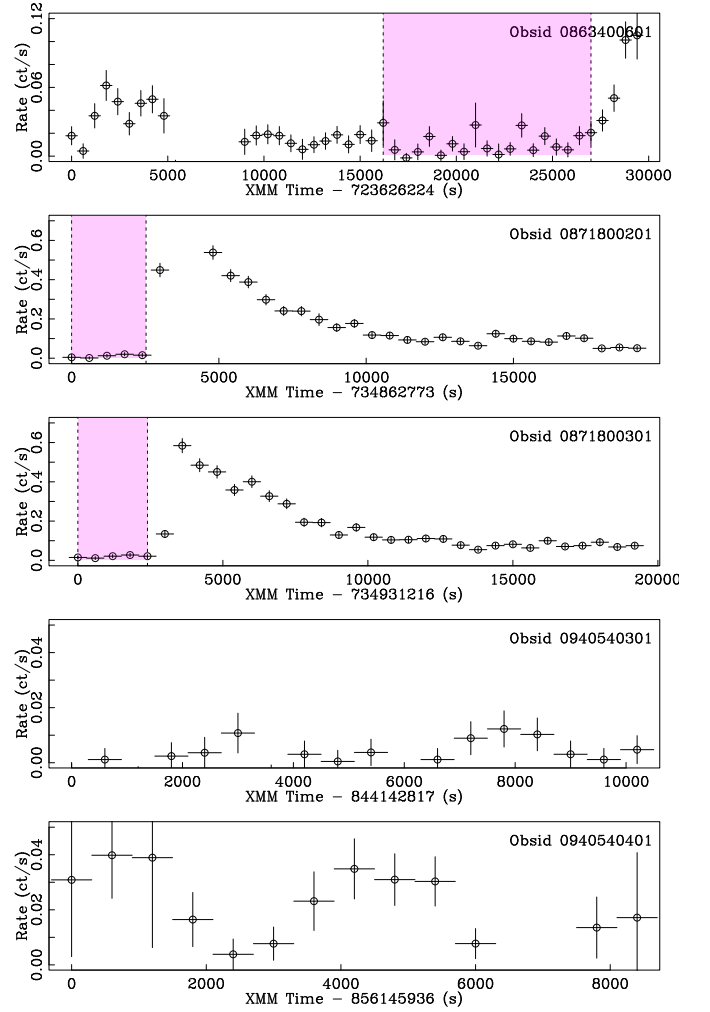


Fig. A.1. Light curves of L 98-59 recorded with the *pn* camera. The shaded areas mark the intervals selected as quiescent phases in the archival observations. For the observations obtained with our program (ObsID 0940540301 and 0940540401) we used the full exposure. For observations 0871800201 and 0871800301 the Y-axis scale is increased to show the entire flares.

from different observations as we did with the wavelet convolution code. We report the ML values in Table 1. The values of ML quantify the detection significance, for L 98-59 they vary in a range between 11.4 and 110.5 among the observations, with the lowest significance due to the faintest emission measured in October 2024.

Appendix B: Optical spectra

Optical spectra of L 98-59 were acquired between October 2018 and April 2019 with ESO HARPS (Cloutier et al. 2019). These spectra encompass the region of CaII H&K lines at 3933 Å and 3968 Å allowing to calculate the S index (Vaughan et al. 1978) and the $\log R'_{HK}$ index (Noyes et al. 1984). Cloutier et al. (2019) report the values of S index derived from the same spectra and that we used to derive $\log R'_{HK}$ with the calibration for M dwarfs given by Astudillo-Defru et al. (2017).

Spectra collected with ESPRESSO spectrograph were acquired between November 2018 and March 2020 allowing a partial overlap with HARPS spectra. We used the data obtained with the ESPRESSO DRS pipeline version 3.2.5 to obtain the S and

Table A.1. Log of the *XMM-Newton* observations of L 98-59.

Observation Identifier	R.A. (J2000)	Dec (J2000)	XMM orbit	Start Date (UT)	P.I.	Time (ks)
863400601	08 18 07.61	-68 18 46.8	3845	2020-12-06 06:27:06.000	Wolk	8.0
871800201	08 18 07.98	-68 18 53.9	3910	2021-04-15 07:42:55.000	France	2.7
871800301	08 18 07.98	-68 18 53.9	3910	2021-04-16 02:43:38.000	France	2.3
940540301	08 18 07.61	-68 18 46.8	4544	2024-10-01 03:16:59.000	Pillitteri	9.7
940540401	08 18 08.07	-68 18 55.6	4614	2025-02-16 22:19:03.000	Pillitteri	4.7

Notes. The last column lists the quiescent time or the good time intervals (GTI) recorded by the *pn* instrument.

$\log R'_{\text{HK}}$ indexes. The 5% – 95% quantile range of $\log R'_{\text{HK}}$ is from -5.6 to -5.2 with a median value of -5.4 . A Lomb-Scargle periodogram of the series of the $\log R'_{\text{HK}}$ index shows a prominent peak at ~ 100 days which likely arises from an alias of the seasonal sampling window and the rotational period of the star (80 days). However, there is no evidence of a long-term cycle in the chromospheric activity indicators.